Editors' Suggestion

Electron-nuclear coherent spin oscillations probed by spin-dependent recombination

S. Azaizia,[1] H. Carrère,[1] J. C. Sandoval-Santana,[2] V. G. Ibarra-Sierra,[2] V. K. Kalevich,[3] E. L. Ivchenko,[3] L. A. Bakaleinikov,[3] X. Marie,[1] T. Amand,[1] A. Kunold,[4] and A. Balocchi[1,*]

[1]*Universitè de Toulouse, INSA-CNRS-UPS, LPCNO, 135 avenue de Rangueil, 31077 Toulouse, France*

[2]*Departamento de Física, Universidad Autónoma Metropolitana Iztapalapa, Avenida San Rafael Atlixco 186, Colonia Vicentina, 09340 Mexico City, Mexico*

[3]*Ioffe Physical-Technical Institute, 194021 St. Petersburg, Russia*

[4]*Área de Física Teórica y Materia Condensada, Universidad Autónoma Metropolitana Azcapotzalco, Avenida San Pablo 180, Colonia Reynosa-Tamaulipas, 02200 Mexico City, Mexico*

(Received 1 March 2018; published 5 April 2018)

We demonstrate the triggering and detection of coherent electron-nuclear spin oscillations related to the hyperfine interaction in Ga deep paramagnetic centers in GaAsN by band-to-band photoluminescence without an external magnetic field. In contrast to other point defects such as Cr^{4+} in SiC, Ce^{3+} in yttrium aluminum garnet crystals, nitrogen-vacancy centers in diamond, and P atoms in silicon, the bound-electron spin in Ga centers is not directly coupled to the electromagnetic field via the spin-orbit interaction. However, this apparent drawback can be turned into an advantage by exploiting the spin-selective capture of conduction band electrons to the Ga centers. On the basis of a pump-probe photoluminescence experiment we measure directly in the temporal domain the hyperfine constant of an electron coupled to a gallium defect in GaAsN by tracing the dynamical behavior of the conduction electron spin-dependent recombination to the defect site. The hyperfine constants and the relative abundance of the nuclei isotopes involved can be determined without the need of an electron spin resonance technique and in the absence of any magnetic field. Information on the nuclear and electron spin relaxation damping parameters can also be estimated from the oscillation amplitude decay and the long-time-delay behavior.

DOI: 10.1103/PhysRevB.97.155201

I. INTRODUCTION

Electron and nuclear spins of well-isolated point defects in semiconductors are excellent candidates for understanding fundamental spin-coupling mechanisms and are a model system for quantum information processing. The coupling through hyperfine interaction (HFI) represents a key spin mechanism in semiconductor systems: responsible for creating mixed electron-nuclear spin states, it has been shown to be useful, e.g., for electron-nuclear spin transfer, in controlling the electron spin coherence time of P donor sites in Si [1–6], and the nitrogen-vacancy centers in diamond [7–16]. The HFI is, however, also responsible for electron and nuclear spin relaxation and decoherence [17].

Similar to nitrogen in diamond, on the one hand, and to shallow defects in silicon, on the other hand, interstitial Ga_i^{2+} defects in the dilute nitride GaAsN [18,19] unite the characteristics of deep and well-isolated paramagnetic centers with an electrically and optically addressable semiconducting system, leading, e.g., to the giant spin-dependent photoconductivity effect [20,21]. The incorporation of nitrogen in (In)GaAs gives rise to paramagnetic interstitial centers composed of a Ga_i^{2+} atom and a single resident electron [19]. These defect sites are at the origin of a very efficient spin-dependent recombination of conduction-band (CB) electrons. This has proven to be an effective tool for, for instance, generating an exceptionally high spin polarization (up to ∼100%) of free and bound electrons in these nonmagnetic dilute nitride semiconductors at room temperature [22–25].

Optically or electrically detected magnetic resonance techniques are consistently employed for manipulating and probing defect spins through the hyperfine interaction and also to identify the defect chemical nature [26,27]. Optically detected magnetic resonance, a variation of nuclear resonance techniques, has been demonstrated on Cr^{4+} impurity ensembles in SiC and GaN [28]. Mostly due to the weak magnetization of nuclear spins, these methods have very low sensitivity. Furthermore, attempts to improve the detection involve high magnetic fields and cryogenic temperatures. Time-resolved Faraday rotation has been successfully used to monitor the $5d$ electron spin time evolution of Ce^{3+} point defects in yttrium aluminum garnet crystals [29]. These techniques partly rely on the spin polarization of electrons bound to centers by coupling the spin states and the electromagnetic field via the spin-orbit interaction occurring in orbitals other than s. Despite the many similarities, in this regard, Ga_i^{2+} centers are fundamentally different. The $4s$ electron spin in Ga_i^{2+} point defects, unlike the $5d$ electron spin in Ce^{3+}, is not directly coupled to the electromagnetic field. However, in these centers CB electrons recombine according to their spin orientation, dynamically polarizing the bound-electron spins. This spin-dependent recombination process, which basically relies on the Pauli exclusion principle, not only can be used to spin polarize the bound electron and to control the degree of nuclear spin polarization [30] but can also be exploited to sense the electron spin dynamics with a time resolution of about 10 ps.

*Corresponding author: andrea.balocchi@insa-toulouse.fr

In this paper we demonstrate an all-optical triggering and detection experiment based on a pump-probe scheme to monitor the bound-electron spins in Ga_i^{2+} centers in the temporal domain. Taking advantage of the spin-dependent recombination mechanisms, we are able to directly trace the hyperfine dynamical features [30]. With the aid of a model based on the master-equation approach for the density matrix of the electron-nuclear spin system, the contribution of at least two different Ga isotopes is established. Also, a comparison of the model calculations with the recorded experimental data reveals the most important parameters involved in the electronic and nuclear spin dynamics of Ga_i^{2+} centers. In the low-power regime, at zero magnetic field, the model yields closed expressions for the photoluminescence intensities that enable us to readily estimate the hyperfine constants and the nuclear and electron spin relaxation damping parameters of the participating isotopes. To gain a better grasp of the interplay between the many spin-related mechanisms in Ga_i^{2+} centers we collect data under a weak magnetic field (65 mT). By self-consistently comparing the retrieved results with the calculations from the developed model, we are able to uncover how the HFI interacts with the sources of spin loss to manipulate them to our advantage. The detection method developed here and the spin mechanisms that it uncovers in Ga centers offer new pathways in the design of all-optical techniques to prepare and monitor the time evolution of electronic and nuclear spins implemented in similar paramagnetic point defects in semiconductor materials.

II. EXPERIMENT

The sample under study consists of a 100-nm-thick $GaAs_{1-x}N_x$ epilayer ($x = 0.021$) grown by molecular beam epitaxy on a (001) semi-insulating GaAs substrate and capped with 10 nm of GaAs. The sample has been investigated at 4 K using the optical orientation technique, which relies on the successive transfer of the angular momentum of the exciting photons, using circularly polarized light, to the photogenerated electrons [31] and finally to the Ga_i^{2+} nuclei. The excitation source is a mode-locked Ti:sapphire laser emitting at an 850-nm split into pump and probe pulses of equal intensity, 1.2-ps duration, and 80-MHz repetition rate. The sample is excited by focusing the pump and probe pulses on the same 50-μm-diameter spot. We should also state here that we work away from spin-dependent recombination (SDR) saturation in order to properly observe the effects [21]. The two-pulse relative time delay Δt is controlled by an optical delay line, and the pulse polarizations are independently set by a system of polarization optics. In order to evidence the HFI features, we have measured the photoluminescence (PL) intensity induced by a circularly polarized probe pulse as a function of (i) the time delay between pump and probe pulses and (ii) the helicity of the pump pulse. In the following, we plot the influence of the pump-pulse helicity on the probe-pulse PL intensity I_{PL}^{pr} by computing the ratio

$$R(\Delta t) = \frac{I_{PL}^{\mathrm{pr}}(\sigma^+,\sigma^+,\Delta t)}{I_{PL}^{\mathrm{pr}}(\pi,\sigma^+,\Delta t)}, \tag{1}$$

where the notation $(\sigma^+/\pi,\sigma^+,\Delta t)$ indicates, respectively, the polarization of the pump pulse, the polarization of the probe pulse (circular σ_+ or linear π), and their respective delay time. No dynamical polarization of the electron-nuclear spin system (ENSS) is expected when the pump is linearly polarized [18]. At long delay times (i.e., when $\Delta t > \tau_{\mathrm{d}}$, where τ_{d} represents the decay time of the CB free carriers) $R(\Delta t)$ probes the ENSS spin memory since all the carriers have recombined. For the measurements at short delay times ($\Delta t \leqslant 100$ ps, for which the PL intensities of the two pulses may partially overlap) the intensity of the probe pulse has been modulated by a mechanical chopper, and its PL intensity has been measured with a photodiode connected to a lock-in amplifier. For larger delay times, a S1 photocathode streak camera coupled to an imaging spectrometer has been employed.

III. RESULTS

We begin by focusing on the zero-magnetic-field case. Figure 1(a) (symbols) presents $R(\Delta t)$ measured for an excitation power $P_{exc} = 4$ mW. The trace presents an oscillating behavior showing that I_{PL}^{pr} can be periodically amplified or reduced by adjusting the delay time Δt when the pump pulse is circularly polarized. For longer delay times the oscillations lose visibility, and a monotonous decrease of the amplifying effect is observed. Figures 1(b) and 1(c) display I_{PL}^{pr} spectra recorded at two extreme points of the oscillations where the probe PL intensity is weakly modified ($\Delta t = 150$ ps) or only strongly increased ($\Delta t = 250$ ps). Below we show that the oscillating and decay features of $R(\Delta t)$ can be directly linked to the coherent oscillations of the electron-Ga system induced by the hyperfine interaction.

The principle of the observation is described in terms of the scheme depicted in Fig. 2 and is based on the following considerations. The HFI Hamiltonian $\hat{H}_{HFI} = \mathcal{A}\hat{\boldsymbol{I}} \cdot \hat{\boldsymbol{S}}_c$ of Ga defects with spin $I = 3/2$ and a single trapped electron of spin $S_c = 1/2$ (where $\mathcal{A}$ is the hyperfine interaction constant) leads to split triplet-quintet eigenstates at zero magnetic field,

$$|J,M\rangle = \sum_{s,m} C_{s,m,M}^{\frac{1}{2},\frac{3}{2},J} |s,m\rangle, \tag{2}$$

where $C_{s,m,M}^{\frac{1}{2},\frac{3}{2},J}$ are the Clebsch-Gordan coefficients, with $m = \pm 1/2, \pm 3/2$ and $s = \pm 1/2$ being the nuclear and electron spin projections on the z axis, respectively, and $M = -J, \ldots, J$ with total spin $J = 1,2$. The splitting between $J = 1$ and $J = 2$ multiplets is $2\mathcal{A}$. Before illumination by the pump pulse, the eight hyperfine states of the ENSS are statistically equipopulated in our experimental conditions (Fig. 2, left panel). The preparation of the defect spin polarization by the pump pulse proceeds as follows: A left-handed circularly polarized pump above the band gap creates preferentially spin-up CB electrons, whereas holes quickly lose their spin orientation and are considered to be unpolarized [32]. The CB electrons are very rapidly captured by the Ga^{2+} interstitial defects ($\tau_e \lesssim 10$ ps), forming a two-electron spin singlet [19,33]: the hyperfine coupling is now *off*. A fast recombination of one of the two defect electrons with an unpolarized hole follows. Due to the photogeneration of CB electron spin polarization, the spin-dependent recombination statistically drives the defect electrons to the same average spin orientation as the conduction-band electrons [18,34]. The recombination

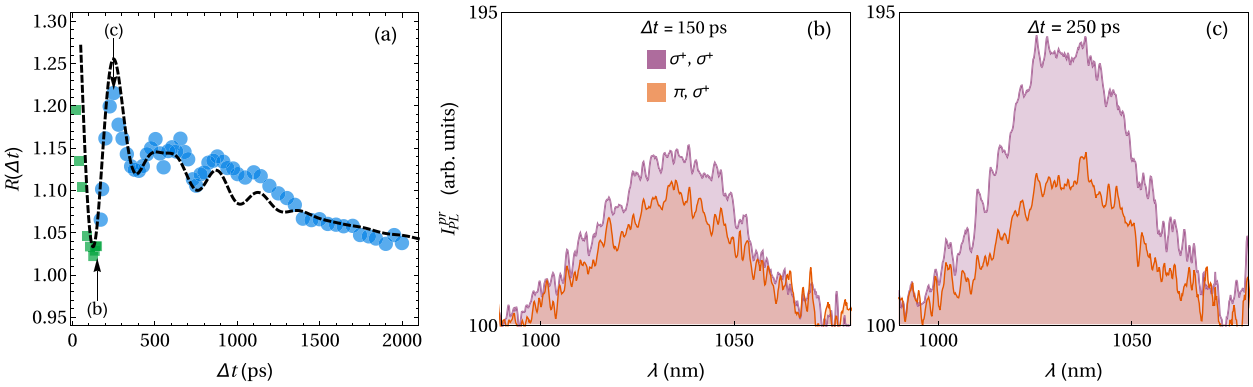

FIG. 1. (a) The ratio of the probe pulse PL intensity under a circularly to linearly polarized pump pulse $R(\Delta t)$ measured as a function of the delay time Δt. Blue circles (green squares) represent the data measured with the streak camera (photodiode) setup. The black dashed line is a fit to the data according to Eq. (12). (b) and (c) The PL intensities induced by the circularly polarized probe pulse after a circularly (purple area) or linearly (orange area) polarized pump pulse at two different delay times marked in (a).

of one of the center paired electrons with an unpolarized hole is fast, typically occurring on the timescale $\tau_h \sim 30$ ps [18,19,35], after which the HFI is reestablished. At the reestablishment of the HFI the remaining electron spin state is projected onto the total spin eigenstates $|J,M\rangle$, leaving the defects in a statistical mixture of states between the $J=1$ and $J=2$ hyperfine levels as $\tau_h 2\mathcal{A}/\hbar \ll 1$, thus triggering the oscillations of the ENSS. Second, the timescale of the recombination ensures as well a relatively constant phase among the ensemble of defect centers. At this point, the quantum system periodically oscillates between the $J=1$ and $J=2$ states, which results in S_{cz} oscillations between the $\pm 1/2$ states. With HFI energy $2\mathcal{A} \sim 15$ μeV [26], the defect preparation time is sizably shorter than the oscillation period $T = h/2\mathcal{A} \sim 250$ ps. The probe beam (Fig. 2, right panel) can now encounter two extreme situations depending on the delay time. In the first case (probe 1) the majority of the defect electrons have the same average spin orientation as the CB ones, preventing the capture. The PL intensity is thus enhanced. In the second case (probe 2), the majority of the defect electrons have an average spin orientation opposite that of the CB electrons, favoring the capture: the PL is now reduced as the conduction band is depleted. If, however, the pump pulse is linearly polarized, no dynamical polarization of the center electron can occur, and the probe-pulse spin-dependent recombination will be insensitive to the delay time. A key feature is that this all-optical approach does not require any external magnetic field, which might modify the spin relaxation damping parameters. Let us now turn our attention to the kinetics of photoelectrons excited by the probe pulse in the conduction band. We can get a qualitative and analytical understanding of the oscillating behavior of $R(\Delta t)$ according to the following argument. Neglecting the electron spin relaxation, the CB electron rate equations can be described by

$$\begin{aligned} \frac{dn_+}{dt} &= -2c_n n_+ N_- - \gamma_r n_+ p, \\ \frac{dn_-}{dt} &= -2c_n n_- N_+ - \gamma_r n_- p, \end{aligned} \tag{3}$$

where $n_\pm(t)$ are the densities of the conduction photoelectrons with spin up (+) and down (−) excited by the probe pulse arriving with the delay time Δt. The CB electron-trapping rate

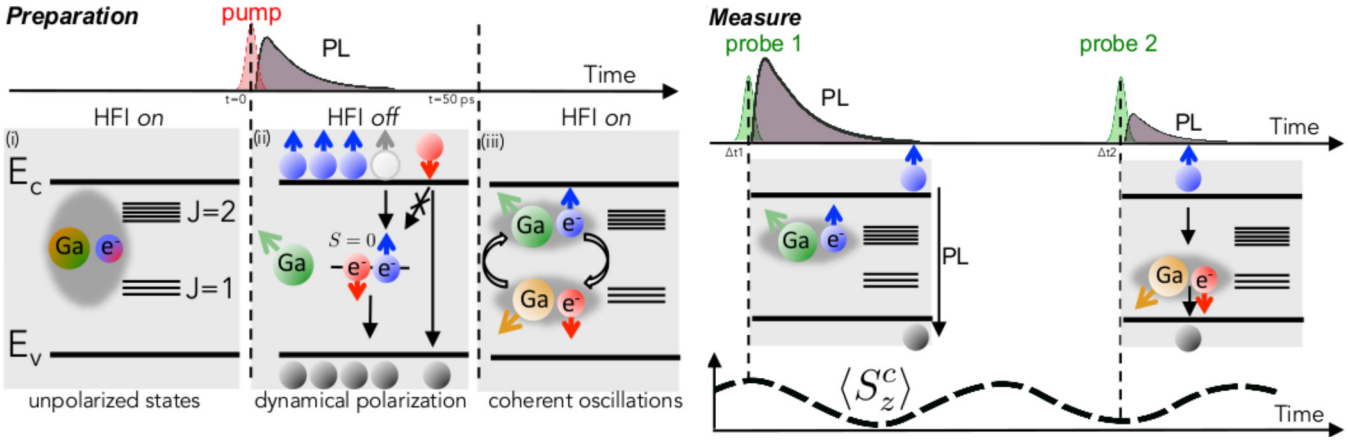

FIG. 2. Schematic representation of the paramagnetic defect nuclear and electron spin oscillation detection scheme. The defect electron arrows indicate the orientation of the average spin $S_{cz} = \langle \hat{S}_{cz} \rangle$ projections. Left: preparation of the coherent oscillations with left-handed circularly polarized pulse. Right: illustration of two extreme situations encountered by the probe beam copolarized with the pump as described in the text.

by paramagnetic centers is given by c_n, p is the hole concentration, and γ_r is the bimolecular recombination constant. The concentrations of single-electron defects $N_\pm$ with an electron spin of $\pm 1/2$ satisfy $N_+ + N_- = N_1$, where N_1 is the density of the centers with one electron. The densities N_+ and N_- are different if the initial pump pulse is circularly polarized and coincide for a linearly polarized pump excitation. Since (i) the electron capture is much more effective than the interband recombination and (ii) $N_\pm$ vary slowly within the capture time $(c_n N_\pm)^{-1}$, the time dependence of $n_\pm$ is described by $n_\pm^{\rm pr} \exp[-2c_n N_\mp(\Delta t)t]$, where $n_\pm^{\rm pr}$ are the conduction electron densities injected by the probe pulse. For a sufficiently weak photoexcitation the measured ratio (1) is described by

$$R(\Delta t) - 1 \propto (n_+^{\rm pr} - n_-^{\rm pr})[N_+(\Delta t) - N_-(\Delta t)]. \quad (4)$$

For circularly polarized pump pulses the values $N_\pm(\Delta t)$ consist of the oscillating and nonoscillating parts,

$$N_\pm(\Delta t) = N_{\pm,0} \pm \frac{\delta N}{2}\cos(\Omega \Delta t), \quad (5)$$

where $\hbar\Omega = 2\mathcal{A}$ is the hyperfine splitting between the electron-nuclear spin quintet and triplet with angular momenta $J = 2$ and $J = 1$, respectively.

The oscillating time behavior of $N_\pm(\Delta t)$ can be understood in terms of the spin-density-matrix approach. In equilibrium the spin density of single-electron defects $\rho_{J',M';J,M}$ is diagonal with equally populated sublevels: $\rho_{J',M';J,M} = (N_1/8)\delta_{J'J}\delta_{M'M}$. The pump pulse generates CB photoelectrons with densities $n_\pm^{\rm pm}$; assuming that the experiment is performed away from SDR saturation, the condition $n^{\rm pm} < N_c$ is satisfied. These photoelectrons are immediately captured by single-electron defects according to Eqs. (3) and form the electron pair states with density $N_2 = n_+^{\rm pm} + n_-^{\rm pm}$. The remaining single-electron defects acquire spin polarization. Immediately after the pulse, i.e., at $\Delta t = 0$, one has $N_\pm(0) = N_c/2 - n_\mp^{\rm pm}$, where $N_c = N_1 + N_2$ is the total density of the deep paramagnetic centers. This equation can be rewritten as

$$N_\pm(0) = \sum_m \rho_{\pm\frac{1}{2},m;\pm\frac{1}{2},m}(0) \quad (6)$$

in terms of the spin-density matrix $\rho_{s',m';s,m}(0) = \delta_{s's}\delta_{m'm}(N_c/8 - n_{-s}^{\rm pm})$ taken in the basis $|s,m\rangle$. In the basis $|J,M\rangle$ we have

$$N_\pm(0) = \sum_{mJ'J} D_{J',J;\pm 1/2,m}\rho_{J',m\pm\frac{1}{2};J,m\pm\frac{1}{2}}(0), \quad (7)$$

where $D_{J',J;s,m} = C^{\frac{1}{2}\frac{3}{2}J'}_{s,m,s+m}C^{\frac{1}{2}\frac{3}{2}J}_{s,m,s+m}$. The components $\rho_{J',M;J;M}(0)$ can be readily expressed via $N_c, n_+^{\rm pm}$ and $n_-^{\rm pm}$. Among these components there are those with $J' = J$ and $J' \neq J$. Neglecting the spin relaxation, we have

$$\rho_{J',M;J,M}(\Delta t) = \rho_{J',M;J,M}(0)e^{-i\Omega(J'-J)\Delta t}. \quad (8)$$

Therefore, the oscillating part of Eq. (5) is contributed by the off-diagonal spin-matrix components with $J' \neq J$. A straightforward calculation gives

$$N_{+,0} - N_{-,0} = \tfrac{3}{8}(n_+^{\rm pm} - n_-^{\rm pm}), \quad (9)$$

$$\delta N = \tfrac{5}{8}(n_+^{\rm pm} - n_-^{\rm pm}). \quad (10)$$

TABLE I. The hyperfine interaction constants for the two naturally stable isotopes of gallium in the four different interstitial configurations occurring in dilute nitrides (In)GaAsN [26].

	Ga_i location			
	A	B	C	D
$\mathcal{A}_1$ (^{69}Ga; $\times 10^{-4}$ cm^{-1})	745	1230	620	580
$\mathcal{A}_2$ (^{71}Ga; $\times 10^{-4}$ cm^{-1})	968.5	1562	787.4	736.6

The last terms on the left-hand sides of Eqs. (3) describe the radiative recombination and the PL intensity. Retaining all the factors, we can present Eq. (4) in the final form

$$R(\Delta t) - 1 = \alpha + \beta\cos(\Omega\Delta t), \quad (11)$$

where coefficients α and β are, respectively, given by $P_i(N_{+,0} - N_{-,0})/N_c$ and $P_i\delta N/N_c$, with P_i being the initial degree of the pump-induced spin polarization $(n_+^{\rm pm} - n_-^{\rm pm})/(n_+^{\rm pm} + n_-^{\rm pm})$. In the presence of two isotopes, which is the case for Ga atoms, the cosine function in Eq. (11) should be replaced by a sum of two cosine functions with frequencies Ω_1 and Ω_2 and relative abundances f_1 and f_2. Allowance for the spin relaxation results in a multiplication of α by $\exp(-\Delta t/\tau_{sc}^*)$ and of β by $\exp(-\Delta t/T_2^*)$, where $1/\tau_{sc}^* = 1/\tau_{sc} + 1/\tau_{sc}^{(1)}(B_z)$ is the bound-electron spin relaxation time and T_2^* is the decoherence time of electron-nuclear spin oscillation, which is affected by both homogeneous relaxation processes and inhomogeneous broadening of the hyperfine splitting. The bound-electron spin relaxation rate is parametrized by τ_{sc} and $\tau_{sc}^{(1)}$, where, in principle, $1/\tau_{sc}^{(1)}$ can be considered to depend on the magnetic field as a Lorentzian function [23]. The magnetic field dependence of $\tau_{sc}^{(1)}$ is such that for vanishing magnetic fields, where the HFI is dominant, $1/\tau_{sc}^* = 1/\tau_{sc} + 1/\tau_{sc}^{(1)}(0)$. However, for large magnetic fields, when the HFI is overcome by the Zeeman energy ($g_c\mu_B B_z \gg 2\mathcal{A}$) and bound electrons are not allowed to exchange angular momentum with the nucleus due to energy mismatch, $1/\tau_{sc}^* = 1/\tau_{sc}$. Therefore, $\tau_{sc}^{(1)}(0)$ accounts for the bound-electron spin relaxation caused by the angular momentum exchange between bound electrons and surrounding nuclei due to the HFI. Finally, the experimentally determined $R(\Delta t)$ can be quantitatively compared with

$$R(\Delta t) - 1 = \alpha e^{-\Delta t(1/\tau_{sc}^*)} + \beta e^{-\Delta t/T_2^*}[f_1\cos(\Omega_1\Delta t) + f_2\cos(\Omega_2\Delta t)], \quad (12)$$

where the positive values f_1 and f_2 are normalized by the condition $f_1 + f_2 = 1$. According to the mechanism described, the circularly polarized probe pulse will sample the oscillating behavior of the hyperfine coupling instantaneously and at different delay times. We obtain a modulation of the probe beam PL intensity directly tracing the HFI in the time domain. In the case of Ga atoms, the two stable isotopes ^{69}Ga and ^{71}Ga have the relative abundances $f_1 = 0.6018$ and $f_2 = 0.3982$, respectively, and their hyperfine constants differ by a factor of $\mathcal{A}_2/\mathcal{A}_1 = 1.27$. The hyperfine constant (Table I [26]) will, however, depend on the particular defect location, which is determined mainly by growth and annealing conditions. Figure 3 details $R(\Delta t)$ for short delays superposed on a simple beating pattern composed of a sum of simple cosine

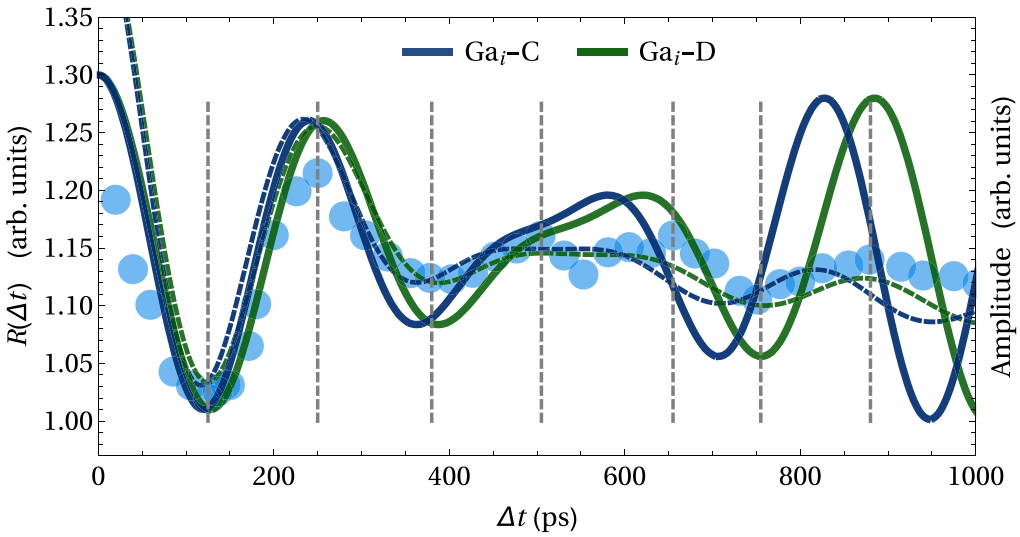

FIG. 3. Detail of the experimental data for short delays (circles) superimposed on simple cosine beat patterns (solid lines) and with damping T_2^* (dashed lines) at the frequencies of two different interstitial configurations. The vertical dashed lines indicate the position of the extrema of the experimental data.

functions at the frequencies of two different Ga interstitial locations. The experimental data present the first destructive interference in the beating pattern in the 500 to 600 ps range. This rules out the occurrence of Ga$_i$-A and Ga$_i$-B as their higher oscillating frequencies are incompatible with this experimental observation. Ga$_i$-C and Ga$_i$-D present very similar hyperfine constants. Nevertheless, the experimental data presented in Fig. 3 allow us to unambiguously identify Ga$_i$-D as the dominant interstitial configuration. Indeed, by fixing the relaxation times $\tau_{sc} = 200$ ns, $\tau_{sc}^{(1)}(0) = 1350$ ps, and $T_2^* = 350$ ns, the fit of Eq. (12) using the experimental data shown in Fig. 1(a) (dashed line) yields $\Omega_1 = 21.8$ GHz, $\Omega_2 = 27.5$ GHz, and $f_1 = 1 - f_2 = 0.59$. In particular, the calculated frequencies $\mathcal{A}_1 = \hbar\Omega_1/2 = 577.8 \times 10^{-4}\,\mathrm{cm}^{-1}$ and $\mathcal{A}_2 = \hbar\Omega_2/2 = 730.6 \times 10^{-4}\,\mathrm{cm}^{-1}$ exhibit good agreement with the hyperfine parameters obtained by optically detected magnetic resonance. This proves that a precise determination of the defect nature and configuration can be obtained by this PL pump and probe scheme [36]. Multiple mechanisms could be responsible for the coherence loss. First of all, the measurement maps the coherent oscillations of the ensemble of Ga centers present under the excitation spot, whose intensity strongly varies from the excitation spot center to the edge. Second, the HFI sampling cannot be considered to be strictly instantaneous but is averaged over the CB electron lifetime τ_{PL}, allowing us only to infer a minimum limit for the coherence time decay. Third, the stochastic nature of the trapping and recombination can also be ascribed as a possible source of coherence loss.

Having determined the most relevant parameters, we now turn to the case where a moderate magnetic field is applied to the sample in the Faraday configuration. Experimental data for

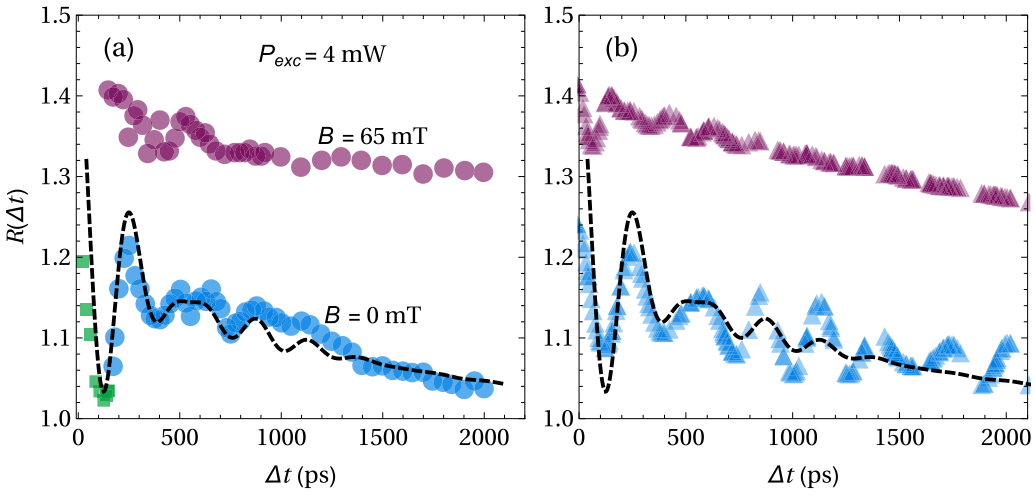

FIG. 4. Spin-dependent recombination ratio $R(\Delta t)$ of the probe pulse as a function of the time delay Δt between the pump and the probe pulses. (a) The experimental results (solid circles) and (b) the calculations obtained from the master equation (solid triangles). Both panels indicate the results for Eq. (12) with dashed lines for $B = 0$.

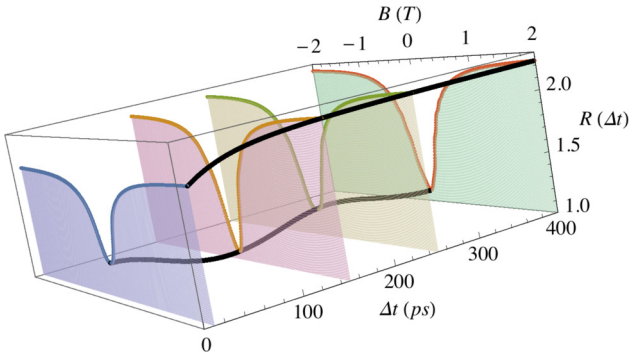

FIG. 5. Spin-dependent recombination ratio $R(\Delta t)$ as a function of a magnetic field in the Faraday configuration for $P_{exc} = 4$ mW and time delays $\Delta t = 10$, 150, 250, and 400 ps.

the time variation of the spin-dependent recombination ratio $R(\Delta t)$ under $B = 65$ mT (purple solid circles) are shown in Fig. 4(a). Making a comparison with the zero-magnetic-field case, three significant differences arise. First, for $B \neq 0$ (purple solid circles) the overall spin-dependent recombination ratio is larger than that for $B = 0$. Second, the beating pattern observed for $B = 0$ nearly vanishes at $B \neq 0$. And third, the relaxation in the $B \neq 0$ case is slower than that of the $B = 0$ case. In general, these observations suggest that the presence of a magnetic field in the Faraday configuration stabilizes the spin polarization of CB electrons. To further investigate this point it would be desirable to extend the validity of Eq. (12) to $B \neq 0$; however, even for moderate magnetic field intensities the picture becomes rather involved. Hence, in order to perform a detailed analysis, we have to resort to the full master-equation approach for the density matrix [30] that accounts for contributions from both Ga isotopes and nuclear spin relaxation due to magnetic dipolar interaction [37–43]. With the parameters determined from the fit of Eq. (12), the dependence $R(\Delta t)$ drawn from the master-equation approach exhibits good quantitative agreement with the experimental results for both cases: $B = 0$ and $B = 65$ mT [see Fig. 4(b)]. Although the fit of Eq. (12) alone yields very good results for the hyperfine parameters, the spin relaxation times are better estimated from the master-equation calculations. The best results were obtained when both approaches were used self-consistently. Figure 5 shows $R(\Delta t)$ induced by the probe pulse as a function of the longitudinal magnetic field at fixed power (4 mW) for various time delays. As the magnetic field increases, $R(\Delta t)$ rises until it saturates for values of the magnetic field whose Zeeman energies are comparable to those of the HFI ($B_{\rm sat} \sim 125$ mT) [24,44]. In full agreement with the results in Fig. 4, $R(\Delta t)$ exhibits higher overall values for $B = 65$ mT. Additionally, the oscillations for $B = 0$ are more pronounced than those of $B > 0$; indeed, they seem to completely vanish for $B \to \infty$. Similar trends have been observed in continuous-wave experiments in the PL degree of circular polarization [23]. To strengthen the argument about the stabilizing effect of the magnetic field, it is instructive to calculate the spin transfer rate due to the HFI $(d\boldsymbol{J}/dt)_{HFI} = \mathcal{A}\langle \hat{\boldsymbol{I}} \times \hat{\boldsymbol{S}}_c \rangle$ between bound electrons and nuclei [34]. Figure 6(a) shows $(d\boldsymbol{J}/dt)_{HFI}$ as a function of time for $B = 0$ (blue solid line) and for $B = 65$ mT (purple solid line). Figure 6(a) presents the overall spin transfer rate as a function of time for a single circularly polarized pulse. The oscillation frequencies of both isotopes, ^{69}Ga and ^{71}Ga, superimpose. The large oscillations (blue solid line) correspond to $B = 0$, and the small ones (purple solid line) correspond to $B = 65$ mT. Figure 6(b) shows the total amount of transferred angular momentum $\int_0^\infty (d\boldsymbol{J}/dt)_{HFI} dt$ as a function of the external Faraday configuration magnetic field. In both panels we consistently observe that the spin transfer between electrons and nuclei is quenched by the presence of a longitudinal magnetic field. We can thus state that at a certain threshold magnetic field strength, the Zeeman interaction exceeds the HFI inhibiting the spin transfer between the bound electrons and nuclei and the electron spin is effectively decoupled from the nuclear one. Since bound electrons possess very long spin relaxation times under such conditions ($\tau_{sc} > 200$ ns), it is clear that, as the magnetic field increases and the HFI is uncoupled by the Zeeman interaction, the spin of bound electrons slowly relaxes due to τ_{sc}. Conversely, when the magnetic field is negligible and,

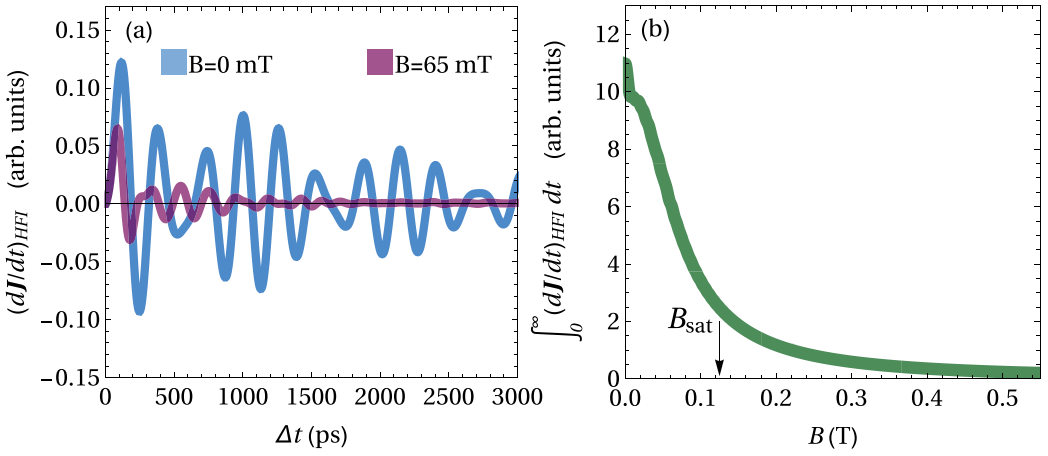

FIG. 6. (a) Spin transfer rate due to the HFI $(d\boldsymbol{J}/dt)_{HFI} = A\langle \hat{\boldsymbol{I}} \times \hat{\boldsymbol{S}}_c \rangle$ as a function of time extracted from the master-equation approach for the ^{69}Ga and ^{71}Ga isotopes. The results for the Faraday configuration magnetic field strength $B = 0$ are shown as a solid blue line, and those for $B = 65$ mT are shown as a solid purple line. The beating is due to the presence of two Ga isotopes. (b) The overall angular momentum transfer $\int_0^\infty (d\boldsymbol{J}/dt)_{HFI} dt$.

consequently, bound electrons and nuclei are strongly coupled by the HFI, bound-electron spins decay faster as their angular momentum is transferred to the rapidly relaxing nuclear spins. The dissipative processes previously introduced in the master equations are basically responsible for the net angular momentum transfer between the center electron and the nucleus observed at zero magnetic field since they irreversibly destroy the coherences in the ENSS at the origin of the oscillations between the average angular momenta of the electron and of the nucleus. In these conditions, Ga centers are less efficient spin filters.

IV. CONCLUSIONS

We have demonstrated that it is possible to trigger and measure the electron-nuclear spin oscillations related to the hyperfine interaction in dilute nitride semiconductor paramagnetic centers by monitoring the band-to-band PL in the absence of any magnetic field. The hyperfine constants and the relative abundances of the nuclei involved can be unambiguously determined without the need of electron spin resonance techniques. Information about the nuclear and electron spin relaxation damping parameters of the paramagnetic center can also be estimated in time domain from the oscillation damping and the long-time-delay behavior. These parameters are direct attributes of the electronic and nuclear spin relaxation mechanisms. Under a moderate magnetic field (65 mT) in the Faraday configuration, the beating pattern, typical of the HFI, is strongly quenched, and the spin-filtering effect becomes more efficient. The bound-electron spins in Ga^{2+} centers are strongly stabilized by the external magnetic field through the Zeeman effect, which decouples it from the nuclear spins and prevents the transfer of angular momentum between the two spins. This multiple-pulse scheme opens new perspectives in time-resolved detection capabilities based solely on the spin-dependent recombination mechanism under zero magnetic field. Even though here we have focused on Ga centers embedded in GaAsN, these methods can easily be adapted to other types of point defects with comparable properties, incorporated in different semiconductors. The spin dynamics revealed by the pump-probe technique developed here provides general guidelines for the desired properties of spin systems based on point defects. We envision that in the future, centers that exhibit spin-dependent recombination mechanisms integrated into a semiconductor matrix with no nuclear spin and, consequently, very slow nuclear spin relaxation will be used to create stable angular momentum states. Using the spin-dependent recombination mechanism presents clear advantages in creating monolithic devices that conjugate the standard electronics with spintronics by coupling spin-polarized CB electrons to the nuclear spins at point defects. The spin state of such systems could be triggered and tracked by the double-pulse method presented here.

ACKNOWLEDGMENTS

We acknowledge funding from LIA CNRS-Ioffe RAS ILNACS. E.L.I. thanks the Russian Foundation for Basic Research (Grants No. 17-02-00383 and No. 17-52-16020). V.K.K. acknowledges the financial support of the government of Russia (Project No. 14.Z50.31.0021). A.K. gratefully appreciates the financial support of Departamento de Ciencias Básicas UAM-A Grants No. 2232214 and No. 2232215. J.C.S.-S. and V.G.I.-S. would like to acknowledge the support received from Becas de Posgrado UAM Scholarships No. 2151800745 and No. 2112800069. X.M. also thanks Institut Universitaire de France. This work was supported by Programme Investissements d'Avenir under the program ANR-11-IDEX-0002-02, reference ANR-10-LABX-0037-NEXT.

[1] B. E. Kane, Nature (London) **393**, 133 (1998).
[2] J. J. Pla, K. Y. Tan, J. P. Dehollain, W. H. Lim, J. J. L. Morton, D. N. Jamieson, A. S. Dzurak, and A. Morello, Nature (London) **489**, 541 (2012).
[3] T. D. Ladd, D. Maryenko, Y. Yamamoto, E. Abe, and K. M. Itoh, Phys. Rev. B **71**, 014401 (2005).
[4] A. Laucht, R. Kalra, J. T. Muhonen, J. P. Dehollain, F. A. Mohiyaddin, F. Hudson, J. C. McCallum, D. N. Jamieson, A. S. Dzurak, and A. Morello, Appl. Phys. Lett. **104**, 092115 (2014).
[5] W. Yao, R.-B. Liu, and L. J. Sham, Phys. Rev. B **74**, 195301 (2006).
[6] V. Ivády, K. Szász, A. L. Falk, P. V. Klimov, D. J. Christle, E. Janzén, I. A. Abrikosov, D. D. Awschalom, and A. Gali, Phys. Rev. B **92**, 115206 (2015).
[7] D. D. Bhaktavatsala Rao, S. Yang, and J. Wrachtrup, Phys. Rev. B **92**, 081301(R) (2015).
[8] S. Zaiser, T. Rendler, I. Jakobi, T. Wolf, S.-Y. Lee, S. Wagner, V. Bergholm, T. Schulte-Herbrüggen, P. Neumann, and J. Wrachtrup, Nat. Commun. **7**, 12279 (2016).
[9] A. Auer and G. Burkard, Phys. Rev. B **93**, 035402 (2016).
[10] T. van der Sar, Z. H. Wang, M. S. Blok, H. Bernien, T. H. Taminiau, D. M. Toyli, D. A. Lidar, D. D. Awschalom, R. Hanson, and V. V. Dobrovitski, Nature (London) **484**, 82 (2012).
[11] N. Mizuochi, P. Neumann, F. Rempp, J. Beck, V. Jacques, P. Siyushev, K. Nakamura, D. J. Twitchen, H. Watanabe, S. Yamasaki, F. Jelezko, and J. Wrachtrup, Phys. Rev. B **80**, 041201 (2009).
[12] J. R. Maze, J. M. Taylor, and M. D. Lukin, Phys. Rev. B **78**, 094303 (2008).
[13] J. J. Pla, F. A. Mohiyaddin, K. Y. Tan, J. P. Dehollain, R. Rahman, G. Klimeck, D. N. Jamieson, A. S. Dzurak, and A. Morello, Phys. Rev. Lett. **113**, 246801 (2014).
[14] Y. Doi, T. Makino, H. Kato, D. Takeuchi, M. Ogura, H. Okushi, H. Morishita, T. Tashima, S. Miwa, S. Yamasaki, P. Neumann, J. Wrachtrup, Y. Suzuki, and N. Mizuochi, Phys. Rev. X **4**, 011057 (2014).
[15] M. W. Doherty, C. A. Meriles, A. Alkauskas, H. Fedder, M. J. Sellars, and N. B. Manson, Phys. Rev. X **6**, 041035 (2016).
[16] K. Nemoto, M. Trupke, S. J. Devitt, A. M. Stephens, B. Scharfenberger, K. Buczak, T. Nöbauer, M. S. Everitt, J. Schmiedmayer, and W. J. Munro, Phys. Rev. X **4**, 031022 (2014).

[17] B. Urbaszek, X. Marie, T. Amand, O. Krebs, P. Voisin, P. Maletinsky, A. Högele, and A. Imamoglu, Rev. Mod. Phys. **85**, 79 (2013).
[18] V. K. Kalevich, E. L. Ivchenko, M. M. Afanasiev, A. Y. Shiryaev, A. Y. Egorov, V. M. Ustinov, B. Pal, and Y. Masumoto, JETP Lett. **82**, 455 (2005).
[19] X. J. Wang, I. A. Buyanova, F. Zhao, D. Lagarde, A. Balocchi, X. Marie, C. W. Tu, J. C. Harmand, and W. M. Chen, Nat. Mater. **8**, 198 (2009).
[20] F. Zhao, A. Balocchi, A. Kunold, J. Carrey, H. Carrère, T. Amand, N. Ben Abdallah, J. C. Harmand, and X. Marie, Appl. Phys. Lett. **95**, 241104 (2009).
[21] A. Kunold, A. Balocchi, F. Zhao, T. Amand, N. B. Abdallah, J. C. Harmand, and X. Marie, Phys. Rev. B **83**, 165202 (2011).
[22] V. K. Kalevich, A. Y. Shiryaev, E. L. Ivchenko, A. Y. Egorov, L. Lombez, D. Lagarde, X. Marie, and T. Amand, JETP Lett. **85**, 174 (2007).
[23] V. K. Kalevich, M. M. Afanasiev, A. Y. Shiryaev, and A. Y. Egorov, Phys. Rev. B **85**, 035205 (2012).
[24] V. K. Kalevich, M. M. Afanasiev, A. Y. Shiryaev, and A. Y. Egorov, JETP Lett. **96**, 567 (2013).
[25] E. L. Ivchenko, L. A. Bakaleinikov, M. M. Afanasiev, and V. K. Kalevich, Phys. Solid State **58**, 1539 (2016).
[26] X. J. Wang, Y. Puttisong, C. W. Tu, A. J. Ptak, V. K. Kalevich, A. Y. Egorov, L. Geelhaar, H. Riechert, W. M. Chen, and I. A. Buyanova, Appl. Phys. Lett. **95**, 241904 (2009).
[27] A. Gruber, A. Dräbenstedt, C. Tietz, L. Fleury, J. Wrachtrup, and C. von Borczyskowski, Science **276**, 2012 (1997).
[28] W. F. Koehl, B. Diler, S. J. Whiteley, A. Bourassa, N. T. Son, E. Janzén, and D. D. Awschalom, Phys. Rev. B **95**, 035207 (2017).
[29] P. Liang, R. R. Hu, C. Chen, V. V. Belykh, T. Q. Jia, Z. R. Sun, D. H. Feng, D. R. Yakovlev, and M. Bayer, Appl. Phys. Lett. **110**, 222405 (2017).
[30] V. G. Ibarra-Sierra, J. C. Sandoval-Santana, S. Azaizia, H. Carrère, L. A. Bakaleinikov, V. K. Kalevich, E. L. Ivchenko, X. Marie, T. Amand, A. Balocchi, and A. Kunold, Phys. Rev. B **95**, 195204 (2017).
[31] F. Meier and B. P. Zakharchenya, *Optical Orientation* (Elsevier, North-Holland, Amsterdam, 1984).
[32] D. J. Hilton and C. L. Tang, Phys. Rev. Lett. **89**, 146601 (2002).
[33] V. K. Kalevich, A. Y. Shiryaev, E. L. Ivchenko, M. M. Afanasiev, A. Y. Egorov, V. M. Ustinov, and Y. Masumoto, Phys. B (Amsterdam, Neth.) **404**, 4929 (2009).
[34] C. Sandoval-Santana, A. Balocchi, T. Amand, J. C. Harmand, A. Kunold, and X. Marie, Phys. Rev. B **90**, 115205 (2014).
[35] D. Lagarde, L. Lombez, X. Marie, A. Balocchi, T. Amand, V. K. Kalevich, A. Shiryaev, E. Ivchenko, and A. Egorov, Phys. Status Solidi A **204**, 208 (2007).
[36] The shorter bound-electron spin relaxation times τ_{sc} observed in the continuous-wave regime [30] can be explained by the higher temperature at which these experiments were performed ($T = 300$ K).
[37] See Supplemental Material at http://link.aps.org/supplemental/10.1103/PhysRevB.97.155201 for a thorough description of the master-equation approach used to model the spin-dependent recombination through the Ga_i-C and Ga_i-D centers.
[38] H. M. Zhao, L. Lombez, B. L. Liu, B. Q. Sun, Q. K. Xue, D. M. Chen, and X. Marie, Appl. Phys. Lett. **95**, 041911 (2009).
[39] R. K. Wangsness and F. Bloch, Phys. Rev. **89**, 728 (1953).
[40] A. G. Redfield, in *Advances in Magnetic Resonance*, Advances in Magnetic and Optical Resonance Vol. 1, edited by J. S. Waugh (Academic, New York, 1965), pp. 1–32.
[41] G. W. Leppelmeier and E. L. Hahn, Phys. Rev. **142**, 179 (1966).
[42] J. Kowalewski and L. Mäler, *Nuclear Spin Relaxation in Liquids: Theory, Experiments, and Applications*, Series in Chemical Physics, edited by J. H. Moore and N. D. Spencer (CRC Press, Boca Raton, FL, 2006), Vol. 128, Chap. 4.
[43] E. L. Ivchenko, V. K. Kalevich, A. Y. Shiryaev, M. M. Afanasiev, and Y. Masumoto, J. Phys.: Condens. Matter **22**, 465804 (2010).
[44] Y. Puttisong, X. J. Wang, I. A. Buyanova, L. Geelhaar, H. Riechert, A. J. Ptak, C. W. Tu, and W. M. Chen, Nat. Commun. **4**, 1751 (2013).